University of California, San Diego UCSD-CER-05-03

# Influence of Particle Location Within Plasma and Focal Volume on Precision of Single-Particle LIBS Measurements

**G. A. Lithgow and S. G. Buckley**

**February 2005**




**Center for Energy Research**
University of California, San Diego
9500 Gilman Drive
La Jolla, CA 92093-0420

# Influence of Particle Location Within Plasma and Focal Volume on Precision of Single-Particle LIBS Measurements

G.A. Lithgow and S.G. Buckley

Department of Mechanical and Aerospace Engineering

University of California, San Diego, 9500 Gilman Drive, MS 0411,

La Jolla, CA 92093-0411; glithgow@ucsd.edu; buckley@ucsd.edu

Corresponding Author:

Prof. Steven G. Buckley

858-534-5681 (phone) / 858-534-5354 (fax)

buckley@ucsd.edu

## Abstract

The effect of the location of particles within the plasma volume on the LIBS signal for single-particle measurements is investigated. Three methods of collecting plasma emission are compared to determine the influence of plasma imaging on particle hit detection rates and signal precision. Imaging larger regions of the plasma volume improves particle detection rates. Spatial integration of the signal from the entire plasma volume tends to reduce uncertainty in the signal caused by variability in the location of particles within the plasma. Additionally, the use of spatially resolved measurements is found to maximize the particle detection efficiency. The use of spatially resolved measurements gives information about the location of particles within the plasma, which

could be used to develop improved hit detection criteria, and to improve the precision of single particle measurements.

Keywords: Laser-Induced Breakdown Spectroscopy; LIBS; plasma spectroscopy; aerosol particle detection

## 1. Introduction

Recently, a number of studies have investigated the use of LIBS for quantitative measurement of single aerosol particles. Particles of interest include exhaust from thermal processes [1], ambient particulate matter [2, 3] and biological aerosols [4-7]. The fact that LIBS is a relatively fast, simple, and inexpensive technique makes it very attractive. When information about individual aerosol particles is desired, ensemble averaging is not useful, so the success of the technique relies on the precision of single-shot measurements.

Recent studies have begun to address the precision of single-shot measurements. Most of this work has focused on shot-to-shot variations in the bulk properties of the laser plasma, such as temperature and electron density. The laser pulse characteristics [8], interactions of the laser pulse with the plasma [9, 10], and interaction of the plasma with particles [11, 12] have all been identified as factors that contribute to shot-to-shot fluctuations of plasma properties.

Additionally, a recent [13] study has shown that the location of individual particles within the plasma volume and the focal volume of the optics can also significantly contribute to uncertainty in the LIBS signal. Multiple spectra were acquired simultaneously from individual laser shots using separate collection optics. The optics

collected light from different regions of the plasma and significantly different LIBS signals were observed. Since each spectrum was taken from the same plasma, the bulk plasma properties were identical, therefore shot-to-shot fluctuations did not contribute to the discrepancy in signals. This implies that the material from ablated particles does not diffuse throughout the volume of the plasma. The atomic emission of the elements of interest is not spatially uniform, and the spatial distribution is not consistent from shot to shot (i.e. there is not simply an optimum location within the plasma).

This study further investigates the role of particle location, and compares three methods of collecting light from the plasma. The previous study demonstrated that when spectra are collected from two regions of a plasma containing a particle, it is possible that one spectrum can record a strong signal, while the other spectrum records no signal. In this study, the effects of imaging larger areas of the plasma on the particle hit rates are investigated. Also, spatially resolved measurements are made to investigate mass transport within the volume, and to develop improved particle detection methods.

## 2. Experimental

### *2.1 LIBS system*

A schematic of the experimental apparatus is shown in Figure 1. The plasma excitation source is a Q-switched Nd:YAG laser operating at the fundamental wavelength (1064 nm), and at 10 Hz, with a pulse width of 10 ns and average pulse energy of 275 mJ. The 10 mm diameter beam is focused with a 75 mm plano-convex fused silica lens. Two sets of optics simultaneously collect plasma emissions into two separate detectors. One set collects emissions at a right angle to the incident laser beam, while the other collects

emissions along the axis of the incident laser beam. Details of the optics are given below in Section 2.2. Each detector system consists of a 0.3 m imaging spectrometer (Acton Research, SpectraPro) with a 1200 G/mm grating, mated to a time-gated ICCD camera (Roper Scientific, PI-MAX). The two cameras are synchronized with a pulse/delay generator (Berkeley Nucleonics) triggered by the laser Q-switch. In this work, the gate delay is 15 μs with respect to the Q-switch and the gate width is 20 μs for each camera.

*2.2 Collection optics and plasma imaging techniques*

Under the given excitation conditions, and at the given delay times, the plasma has a long axis of approximately 5 mm along the laser beam axis, and is approximately 2 mm across in the transverse direction. These dimensions were determined by measuring the integrated continuum plasma emission collected with a single fiber. The fiber was translated across the plasma image, and the limits were defined at the points where emission was no longer visible. More detailed measurements of the plasma dimensions were not undertaken in this study, for full treatment of plasma volume considerations see [14]. Three data sets were acquired (Cases 1, 2, and 3), and in all experiments, plasma emission was collected simultaneously with two sets of optics, one at 90° to the incident laser beam (referred to as the side-collection method), and the other at 180° (referred to as the back-collection method). In each case, the side-collection optics were changed to image the plasma in a different manner, while the back-collection optics were unchanged and used as a reference. In all cases the side-collection optics used two 50 mm diameter, plano-convex, UV-grade fused silica lenses to focus the plasma emission onto a UV fused silica fiber bundle, which guided the light to the entrance slit of the spectrometer.

An iris was placed between the second lens and the fiber to ensure a relatively sharp image of the plasma at the tip of the fiber bundle, restricting the F# to approximately 3.

For Case 1, the two side-collection lenses were identical, each with a focal length of 75 mm, giving a magnification ratio of M = 1. The first lens was placed at a distance from the plasma equal the focal length. A large fiber bundle consisting of 19 fibers of 300 μm core diameter was used, with a total bundle diameter of approximately 2.5 mm. These fibers were not tightly packed, the bundle actually consisted 37 fibers, but only 19 randomly selected fibers were directed to the spectrometer slit. The long axis of the plasma image was significantly larger than the fiber bundle, so the bundle was located at the point of maximum intensity, as measured by the integrated continuum emission.

In Case 2, the first collimating lens was replaced with a 150 mm focal length, 50 mm diameter lens, resulting in M = 0.5. Again, the first lens was placed at a distance from the plasma equal to its focal length. In this case, the length of the plasma image was approximately equal to the bundle diameter, ensuring that light was collected from nearly the entire plasma volume. For each of the first two cases, light from all of the fibers was integrated by binning all rows of the CCD chip.

In Case 3, the M = 1 optics from Case 1 were used to focus the light onto a linear array of 10 optical fibers, each with a core diameter of 500 μm. Light from each fiber was detected separately by binning 10 different regions of the CCD, each region consisting of 15 rows of pixels. In this manner, 10 spectra were collected simultaneously, each from a different region along the major axis of the plasma volume. The placement of each fiber bundle with respect to the plasma image in each case is illustrated in Figure 2.

As a reference, the same optics were used for the back-collection method in all cases. The laser-focusing lens (50 mm diameter, 75 mm focal length, plano-convex, UV grade fused silica) was used to collimate the emission from the plasma. The collimated light was diverted from the laser beam path with a pierced mirror (75 mm diameter mirror, 10 mm hole, enhanced-UV aluminum coating), then focused onto an optical fiber bundle with a second lens (f = 75 mm, d = 50 mm), which launched the light into the spectrometer's entrance slit. The fiber bundle consisted of 7 UV-grade fused silica fibers, each with a core diameter of 200 μm. The total bundle diameter was approximately 700 μm, which was significantly smaller than the plasma image, which was approximately 2 mm in diameter. The bundle was located at the center of the plasma image.

*2.3 Single particle generation and detection*

To make single-particle measurements, a dilute stream of magnesium chloride aerosols was introduced into the LIBS plasma. A high purity $MgCl_2$-water solution was atomized using a commercial pneumatic atomizer (TSI model 3076) and diluted with HEPA filtered air. The particles were size selected by electric mobility diameter using a differential mobility analyzer (TSI model 3080). The mean diameter was 500 μm. The laser plasma sampled the particles in a free jet of the particle-laden flow introduced into open laboratory air.

Conditional data processing, similar to the method developed by Hahn [15, 16], was used to determine whether Mg was detected within the plasma for each shot of the laser. The signal used to quantify the analyte present in the plasma is defined as the integrated atomic line normalized by the continuum baseline value, and termed the peak-

to-base (P/B) ratio. The Mg II lines at 279.6 and 280.3 nm were used in concert to determine the presence of Mg, and a spectrum was considered a hit if the P/B ratios of both lines were higher than threshold values. With no analyte present and signal due only to noise, the two-line criteria resulted in false hit rates of 0.01% or less. The particle stream was diluted so that particle hits occurred between 1% and 5% of the laser shots. Under these conditions, the vast majority of the collected "hit" spectra can be considered to be from plasmas containing single particles, with a small fraction containing more than one particle, and a negligible fraction of false hits. For each laser shot in Case 3, the side-collection system recorded ten spectra simultaneously. P/B ratio thresholds for each channel were determined independently to allow for changing noise signatures in different plasma regions. If any of the ten spectra contained a two-line signal above the threshold, it was considered a hit and all ten spectra were saved.

**3. Results and Discussion**

In a companion study [13], it was demonstrated that the measured LIBS signal can vary significantly depending on the manner in which plasma emission is collected into the detector. When two spectra are collected from a single plasma they often show very different LIBS signals. In extreme cases, one spectra can exhibit a strong LIBS signal while the same element is completely undetectable in the other spectra from the same plasma. This is attributed only to the variation of particle location within the plasma volume, and the relative focal volumes of the collection optics. It was observed in the previous study that the back-collection method had a higher particle hit rate than the side collection method. In that case, each detector was coupled to the optics using an

identical 7-fiber bundle, but the plasma image created by the side collection optics was significantly larger than that created by the back-collection method, so a smaller fraction of the plasma volume was imaged by the side-collection fiber bundle. It was hypothesized that the discrepancy in the hit rates was due to the fact that the side-collection method was collecting light from a smaller region of the plasma, and therefore it was less likely that a particle would be located within the focal volume of the optics.

The relative particle detection rates for the three imaging methods in the present study, as well as the case from the previous study, are given in Table 1. The particle concentrations were not exactly constant for all cases, so only relative hit rates were used as a comparison between cases. It is clear that for the three cases in which a single spectrum was taken from the side, the relative hit rate increases as the imaged area of the plasma increases. Additionally, Case 3 showed the highest hit rate of all methods, detecting almost all of the particles that were detected by either method. The improved detection efficiency of Case 3 over Case 2 is likely due to the fact that the signal is spatially resolved, rather than due to differences in imaged area. Both Case 2 and Case 3 collect light from across nearly the entire plasma image, however, in Case 2 all of the light is integrated together. As a result a weak signal that is localized in a small region gets integrated with pure noise from the rest of the plasma, resulting in an overall signal below the detection threshold. In Case 3, if the localized signal is above the detection threshold at any of the fiber locations, the shot is recorded as a hit.

Ideally, the signals from the side- and back-collection methods would be well correlated since the signals come from the same particles. An observed systematic difference between the two signals is a reflection of the lack of precision between the

imaging. In Figures 3a and 3b, the correlation of the back- and side-colleted signals are shown for Cases 1 and 2 respectively. Each point is a single shot of the laser with the P/B ratio from the side-collected spectrum on the horizontal axis, and the P/B ratio of the back-collected spectrum on the vertical axis. In both, there was very poor correlation between the side-collection and back-collection method, illustrating the limitations of the precision of one or both of the methods.

The masses of individual particles or the distribution of particle masses is not known, so the P/B ratio distributions of the different collection methods cannot be independently verified. This makes comparison of the precision of two collection methods difficult. However, it is expected that the particle masses will have a distribution centered around a value corresponding to the size selected by the DMA. Histograms of the P/B ratios of each particle hit for both the side- and back-collection signals in Cases 1 and 2 are shown in Figure 4 along with the mean and standard deviation of the distribution. In each case, the back collection method shows no clear peak in the distribution, the distributions are truncated at the threshold cutoff value. The side-collection methods both show a distinct peak, and have narrower distributions compared with the back-collected signals. The back-collected distributions, using identical optics, show similar distributions, suggesting that the particle mass distributions are similar for each case. However, there is a notable difference between the side-collected distributions. Case 2, in which a larger area was imaged, shows an even narrower distribution than Case 1. This would suggest that when larger area of the plasma is imaged, the variation in the signal due variability in particle location is reduced.

At first glance, in Cases 1 and 2, the back-collection method appears to give a stronger signal on average than the side-collection method when a particle is detected by each method. This is illustrated in Figure 5, which shows the difference between the P/B ratio for each shot in which a particle was detected by each method for Cases 1 and 2. Positive values on the x-axis reflect spectra pairs with stronger back-collected signals, negative values reflect spectra pairs with stronger side-collected signals. The distribution shows that for any given particle, either method could give a stronger signal, but the distributions are skewed, indicating that the back collection method tends to give a stronger signal. This could indicate that the back collection method tends to collect light from a region of the plasma where conditions tend to favor stronger atomic lines, or weaker continuum emissions, producing a stronger P/B signal. However, this is better explained simply by the difference in imaged area and the fact that ablated material from a particle tends to diffuse a limited distance. With the back-collection method, a smaller area was imaged, so if a particle was located directly in the imaged region, it produced a strong signal. If the particle was located elsewhere, it was simply recorded as a miss, and does not appear in Figure 5. Conversely, when a larger area is imaged, a region of weak signal is integrated along with the strongly emitting region, producing fewer hits with very strong signals, but more hits overall.

In Case 3, spatially resolved measurements were made of single plasmas. Spectra from ten locations along the length of a single plasma image, corresponding to one particle hit, are shown in Figure 6. Each spectra is from a different fiber in the linear array, and contains light from different locations along the length of the plasma. Very strong peaks are visible in spectra 8 and 9, with relatively weaker peaks in spectra 7 and

10, and no visible peaks in the remaining six spectra. The P/B ratio as a function of axial position along the plasma is plotted in Figure 7. A clear maximum is visible in the plot, indicating that the $MgCl_2$ particle was located at the position of peak signal intensity during the plasma formation.

Another particle hit is shown in Figure 8. Again a clear peak in the signal distribution is visible, but at a different location. The variation in Mg signal is not attributed to spatial variations in plasma properties, but rather to variations in the concentration of Mg. It should be noted that the continuum background emission is similar for each shot, indicating that the plasma location, and the position of the fibers relative to the image remain fixed. Plots of the P/B ratio distributions for several particle hits are shown in Figure 9. In most of the hits, a single clear peak is visible, though often it is truncated at the edge of the plasma. In some cases, the signal is distributed across the length of the plasma, indicating that sometimes the ablated material does distribute throughout the plasma volume. In other cases, a more complicated signal distribution is seen. These complicated distributions could be due either to the presence of more than one particle within the plasma volume, or possibly to more complicated mass transport phenomena.

When the ten side-collected spectra of Case 3 are integrated and the resulting P/B ratio compared to the back-collected spectra, the distribution is again skewed towards the back-collection method (Figure 10a). However, if the maximum P/B ratio of the ten spectra is compared to the back-collected spectra, as shown in Figure 10b, the distribution becomes skewed towards the side-collected spectra. This supports the conclusion that the back-collection method does not image an optimum region of the

plasma. When a small region of the plasma is imaged, the signal contains greater variability due to the location of particles, and gives excessively strong signals when particles are located within the imaged region.

These results suggest that the use of spatially resolved measurements could provide a means of improving the precision of single particle measurements. The spatial distribution of the signal gives information about the location of a particle within the plasma, and could be used as a criterion to determine whether the particle was completely vaporized in the plasma, or to reject shots that contain more than one particle. It is expected that proper spatial integration of the signal will also improve the precision of the signal. The spatial integration of the signal should take into account the effective volume imaged by each collected channel as well as spatial variations of plasma properties. Further study using completely monodisperse particles, to remove the uncertainty in particle mass distributions, is necessary to determine a proper signal integration technique.

**4. Conclusions**

This work illustrates the important role that plasma imaging methods play in single particle LIBS measurements. It is shown that ablated material from particles engulfed in the plasma does not diffuse uniformly throughout the plasma volume, and that emission from the particle material is not uniform across the plasma volume. This means that the location of the particle within the focal volume of the collection optics has a significant influence on the resulting LIBS signal. It is clear that when light is collected only from a limited region of the plasma volume, particles within the plasma are often undetected. Increasing the area of the plasma imaged results in improved detection

efficiency. Imaging a larger area of the plasma also reduces the effect of variation of particle location within the plasma and focal volumes, giving improved precision of the measurements.

Using spatially resolved measurements provides a means of further improving single particle measurements. Spatially resolved detection thresholds used in conjunction with a large imaged area is the optimum method for maximizing particle hit detection rates. Spatially resolved measurements also give information about the location of particles within the plasma volume, and the mass transport within the plasma. This information could be used develop more sophisticated particle hit detection criteria, and improved signal precision through proper spatial integration.

**Acknowledgements**

The authors gratefully acknowledge funding from the National Science Foundation Bioengineering and Environmental Systems Early CAREER Development Grant #BES-0349656 and #BES-0093853.

**References**

1. Buckley, S.G., H.A. Johnsen, K.R. Hencken, D.W. Hahn, Laser-Induced Breakdown Spectroscopy as a Continuous Emission Monitor for Toxic Metals in Thermal Treatment Facilities. Waste Man. 20 (2000) 455-462.
2. Carranza, J., B. Fisher, G. Yoder, D. Hahn, On-line Analysis of Ambeient Air Aerosols Using Laser-Induced Breakdown Spectroscopy. Spectrochim. Acta, Part B. 56 (2001) 851-864.

3. Lithgow, G.A., A.L. Robinson, S.G. Buckley, Ambient Measurements of Inorganic Species in an Urban Environment Using Laser-Induced Breakdown Spectroscopy. Atmos. Environ. 38 (2004) 3319-3328.

4. Hybl, J., G.A. Lithgow, S.G. Buckley, Laser-Induced Breakdown Spectroscopy Detection of Biological Material. Appl. Spectrosc. 57 (2003) 1207-1215.

5. Morel, S., N. Leone, P. Adam, J. Amouroux, Detection of bacteria by time-resolved laser induced breakdown spectroscopy. Appl. Optics. 42 (2003) 6184-6191.

6. Boyain-Goitia, A., D.C.S. Beddows, B.C. Griffiths, H.H. Telle, Single-pollen analysis using laser-induced breakdown spectroscopy and Raman microscopy. Appl. Optics. 42 (2003) 6119-6132.

7. Samuels, A., F. DeLucia Jr., K. McNesby, A. Miziolek, Laser-Induced Breakdown Spectroscopy of Bacterial Spores, Molds, Pollens, and Protein: Initial Studies of Discrimination Potential. Appl. Optics. 42 (2003) 6205-6209.

8. Hohreiter, V., J. Carranza, D. Hahn, Temporal analysis of laser-induced plasma properties as related to laser-induced breakdown spectroscopy. Spectrochim. Acta B. 59 (2004) 327-333.

9. Bindhu, C., S. Harilal, M. Tillack, F. Najmabadi, A. Gaeris, Laser propagation and energy absorption by an argon spark. J. Appl. Phys. 94 (2003) 7402-7407.

10. Bindhu, C.V., S.S. Harilal, M.S. Tillack, F. Najmabadi, A.C. Gaeris, Energy Absorption and Propagation in Laser-Created Sparks. Appl. Spectrosc. 58 (2004) 719-726.

11. Carranza, J.D. Hahn, Assessment of the upper particle size limit for quantitative analysis of aerosols using laser-induced breakdown spectroscopy. Anal. Chem. 74 (2002) 5450-5454.

12. Hohreiter, V., A. Ball, D. Hahn, Effects of aerosols and laser cavity seeding on spectral and temporal stability of laser-induced plasmas: applications to LIBS. J. Anal. Atom. Spectrom. 19 (2004) 1289-1294.

13. Lithgow, G.A.S.G. Buckley, Effects of Emission Collection on Single-Particle LIBS Analysis. submitted, Appl. Phys. Lett. (2004).

14. Carranza, J.D. Hahn, Plasma volume considerations for analysis of gaseous and aerosol samples using laser-induced breakdown spectroscopy. J. Anal. Atom. Spectrom. 17 (2002) 1534-1539.

15. Hahn, D.W., W.L. Flower, K.R. Hencken, Discrete Particle Detection and Metal Emissions Monitoring Using Laser-Induced Breakdown Spectroscopy. Appl. Spectrosc. 51 (1997) 1836-1844.

16. Hahn, D.W.M.M. Lunden, Detection and Analysis of Aerosol Particles by Laser-Induced Breakdown Spectroscopy. Aerosol Sci. Tech. 33 (2000) 30-48.

| | Total number of hits detected | # of hits detected only by side-collection | # of hits detected only by back-collection | # of hits detected by both methods | % of total particles detected by back-collection | % of total particles detected by side-collection |
|---|---|---|---|---|---|---|
| Previous Study | 522 | 125 | 177 | 220 | 76% | 66% |
| Case 1 | 1155 | 390 | 261 | 504 | 66% | 77% |
| Case 2 | 1435 | 633 | 191 | 611 | 56% | 87% |
| Case 3 | 684 | 298 | 33 | 353 | 56% | 95% |

Table 1. Relative hit rates for each optical setup.

**Figure captions**

Fig. 1. Schematic of experimental apparatus.

Fig. 2. Location of fiber bundles with respect to side-collected (a) and back-collected (b) plasma image.

Fig. 3. Simultaneous side- and back-collected signals of individual particle hits show poor correlation in both for Case 1 (a) and Case 2 (b).

Fig. 4. In both cases, the single shot peak-to-base ratio distributions from the back-collection method show no clear peak (a,c), while the side-collection method shows a more normal distribution. For the side-collection method, the larger imaged area of Case 2 (d) shows a clearer peak, and a narrower distribution than smaller imaged region of Case 1 (b).

Fig. 5. The strength of simultaneous side- and back-collected signals from individual laser shots tends to show a bias toward the back-collected method. When a larger area is imaged with the side-collection optics in Case 2 (b), the distribution shows a stronger bias towards the back-collected signal than in Case 1 (a).

Fig. 6. Ten spectra collected simultaneously at ten locations across the plasma image. Strong Mg peaks are visible in spectra 7,8,9, and 10. Mg peaks are not present in the remaining 6 spectra.

Fig. 7. The LIBS signal from each of ten spectra plotted as a function of position. The signal shows strong variation across the plasma with a clear maximum.

Fig. 8. Signal variation for a second particle hit, located at a different position than Fig. 7 within the plasma.

Fig. 9. Several particle hits showing different distributions of peak-to-base ratio across the plasma volume.

Fig. 10. The LIBS signal is again skewed towards the back-collection method when compared to the peak to base ratio of the integrated side-collected signal in Case 3 (a). However, when compared to the maximum of the spatially resolved signal, the signal is skewed towards the side-collected measurement (b).

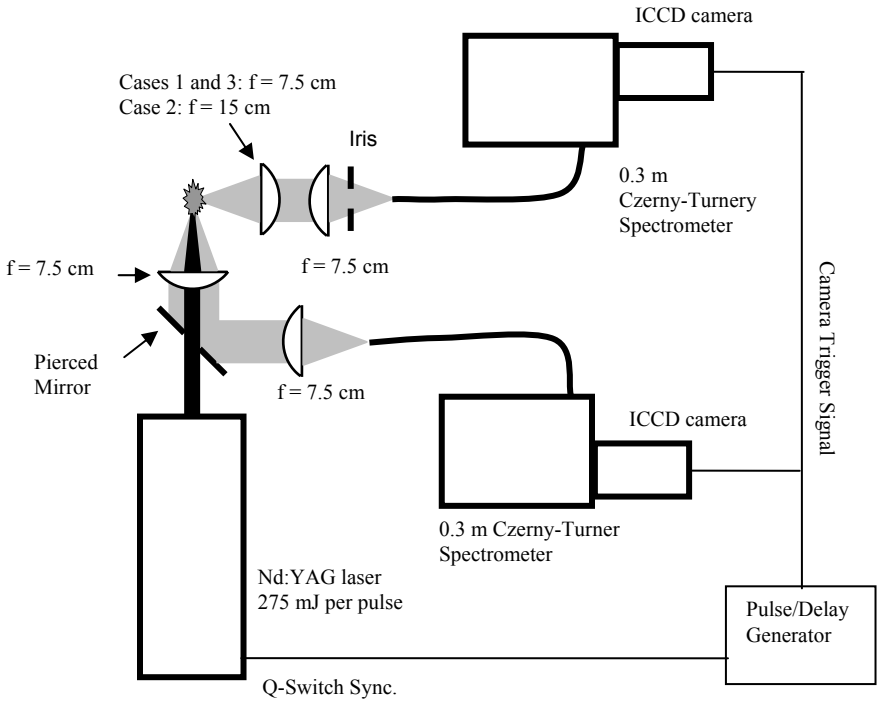
ICCD camera
Cases 1 and 3: f = 7.5 cm
Case 2: f = 15 cm
Iris
0.3 m
Czerny-Turnery
Spectrometer
f = 7.5 cm
f = 7.5 cm
Pierced
Mirror
f = 7.5 cm
ICCD camera
Camera Trigger Signal
0.3 m Czerny-Turner
Spectrometer
Nd:YAG laser
275 mJ per pulse
Pulse/Delay
Generator
Q-Switch Sync.

Figure 1

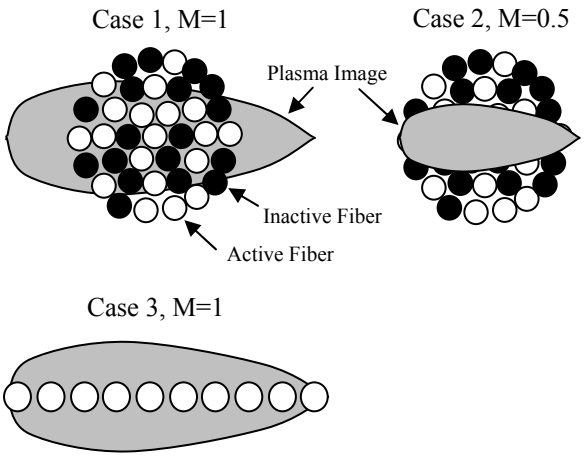


Figure 2 (a)

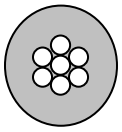

Figure 2 (b)

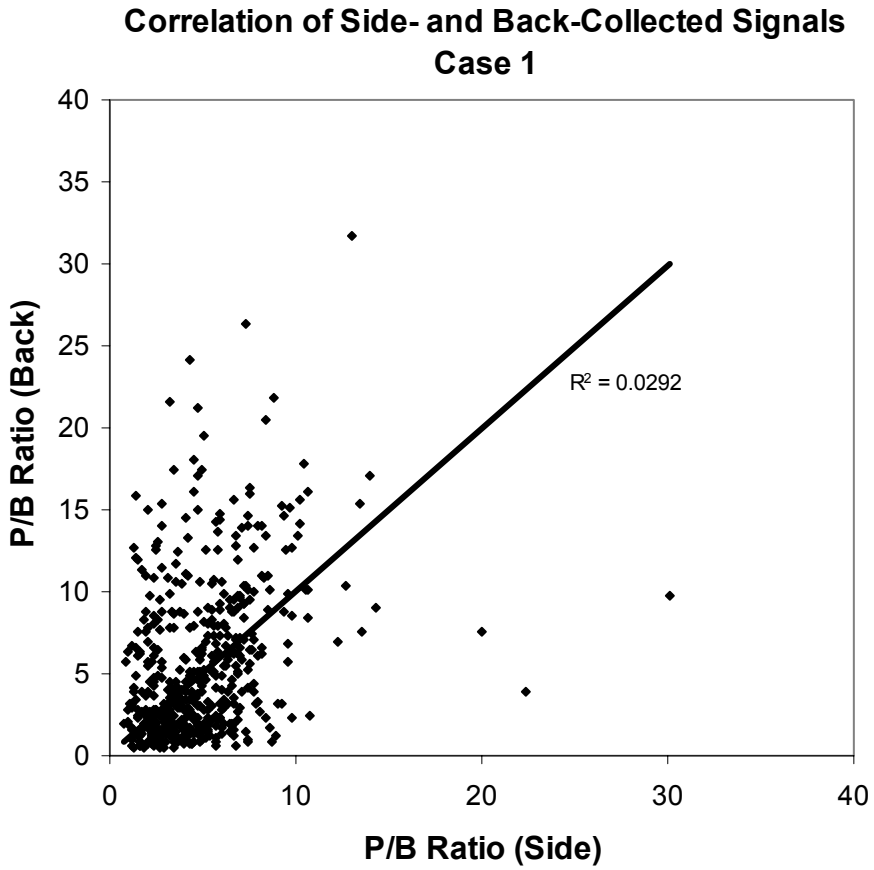
Correlation of Side- and Back-Collected Signals
Case 1
P/B Ratio (Back)
P/B Ratio (Side)
R² = 0.0292
0
5
10
15
20
25
30
35
40
0
10
20
30
40

Figure 3 (a)

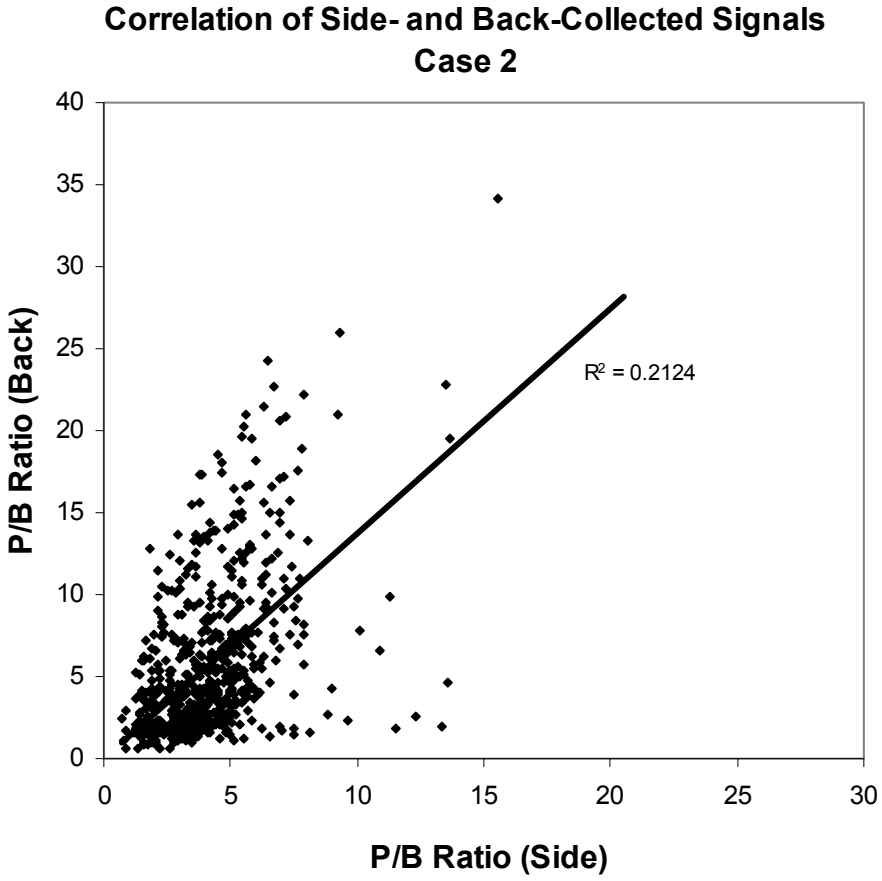
Correlation of Side- and Back-Collected Signals
Case 2
P/B Ratio (Back)
P/B Ratio (Side)
R² = 0.2124
0
5
10
15
20
25
30
35
40

Figure 3(b)

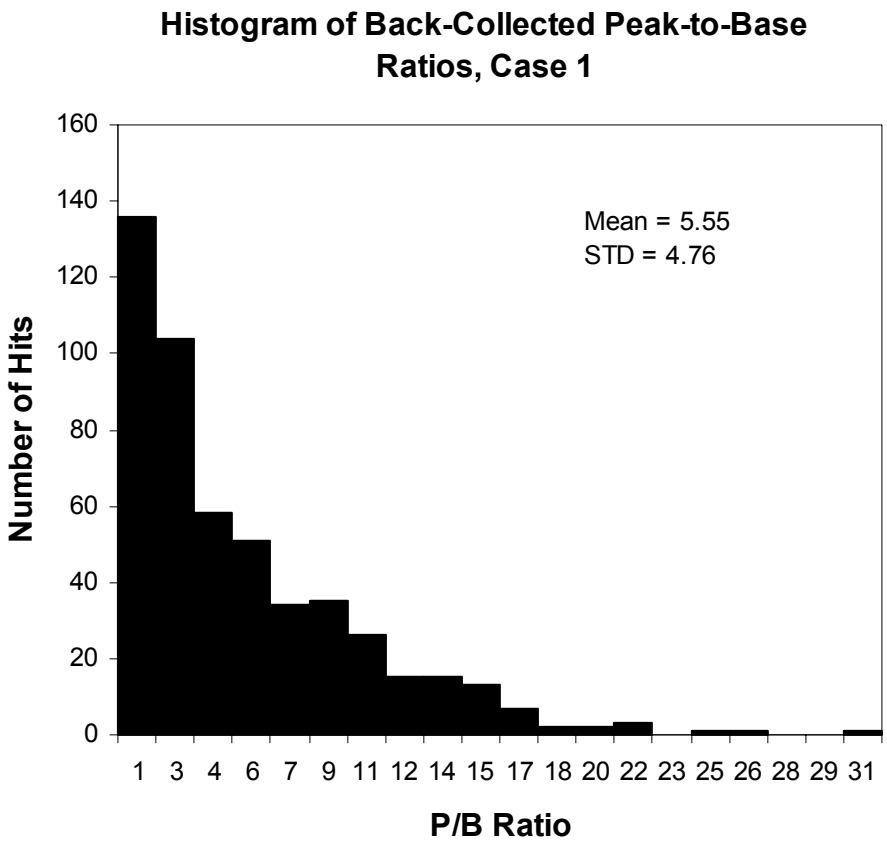
Histogram of Back-Collected Peak-to-Base Ratios, Case 1
Mean = 5.55
STD = 4.76
Number of Hits
P/B Ratio
0
20
40
60
80
100
120
140
160
1 3 4 6 7 9 11 12 14 15 17 18 20 22 23 25 26 28 29 31

Figure 4 (a)

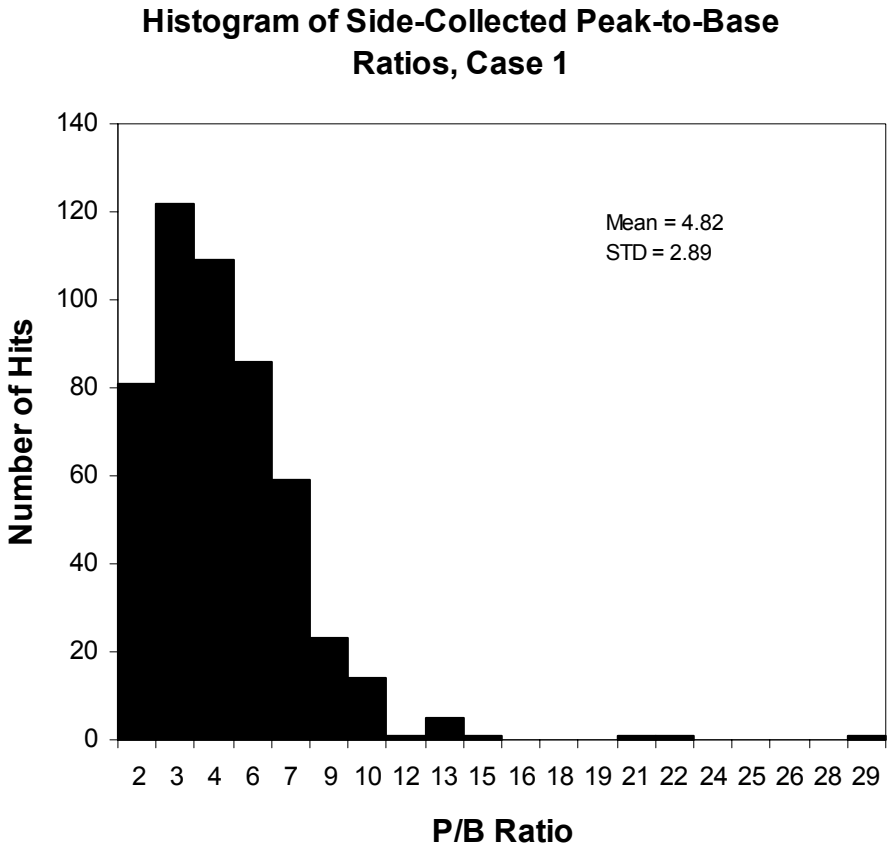
Histogram of Side-Collected Peak-to-Base Ratios, Case 1
Mean = 4.82
STD = 2.89
Number of Hits
P/B Ratio
0
20
40
60
80
100
120
140
2 3 4 6 7 9 10 12 13 15 16 18 19 21 22 24 25 26 28 29

Figure 4 (b)

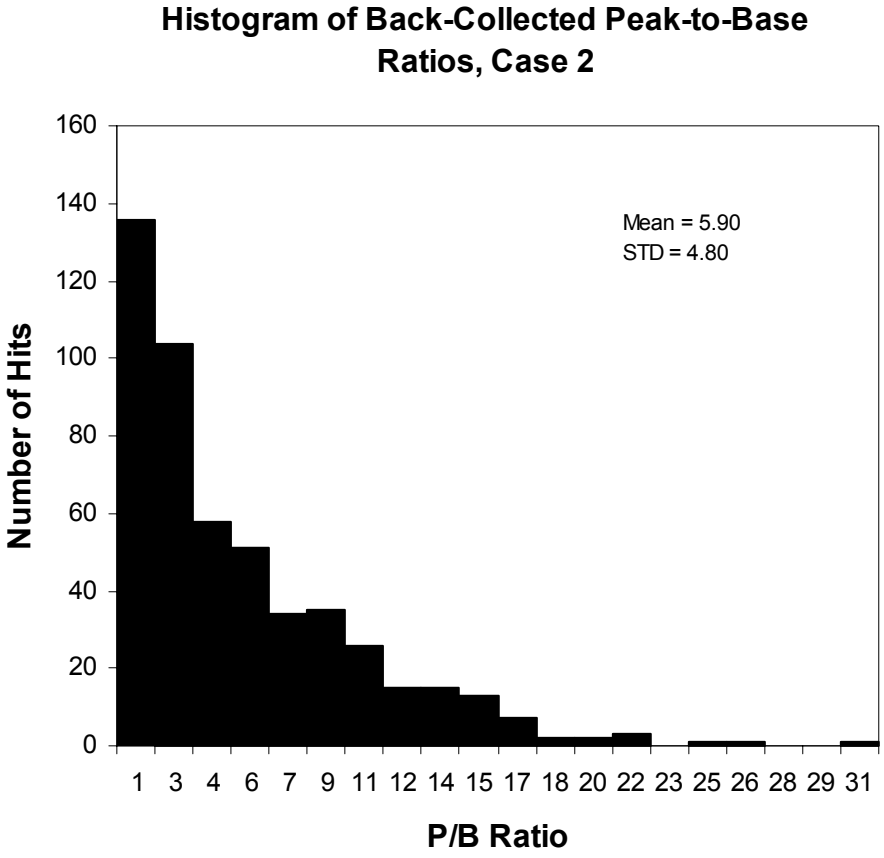
Histogram of Back-Collected Peak-to-Base Ratios, Case 2
Mean = 5.90
STD = 4.80
Number of Hits
P/B Ratio
0
20
40
60
80
100
120
140
160
1 3 4 6 7 9 11 12 14 15 17 18 20 22 23 25 26 28 29 31

Figure 4 (c)

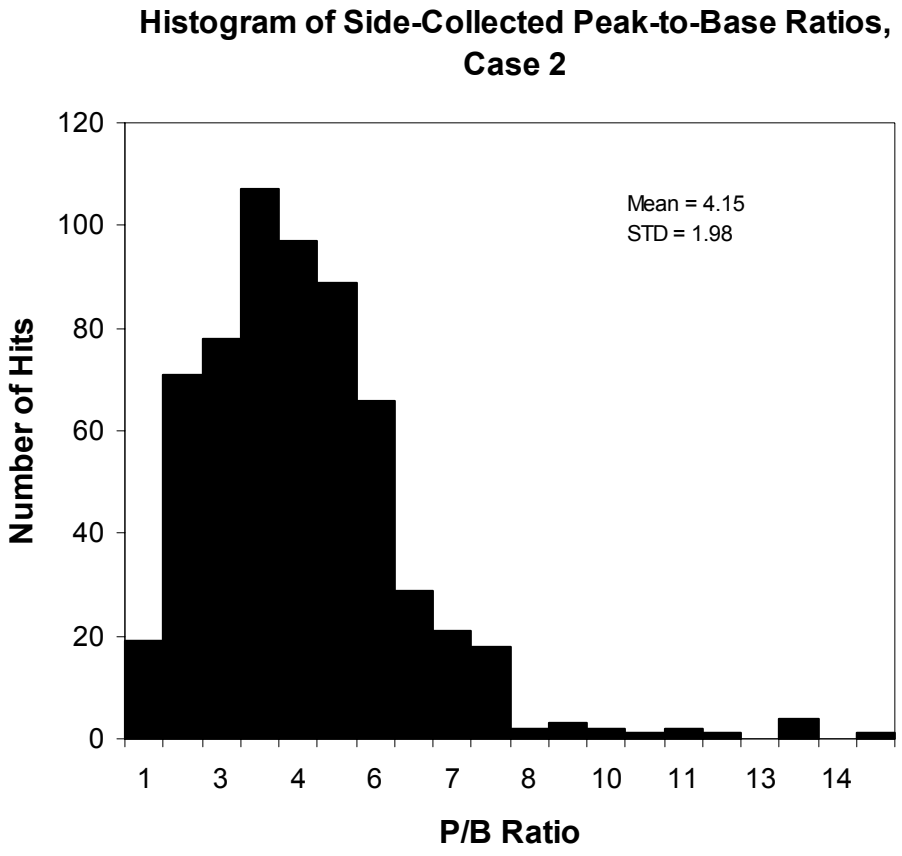
Histogram of Side-Collected Peak-to-Base Ratios, Case 2
Mean = 4.15
STD = 1.98
Number of Hits
120
100
80
60
40
20
0
1
3
4
6
7
8
10
11
13
14
P/B Ratio

Figure 4 (d)

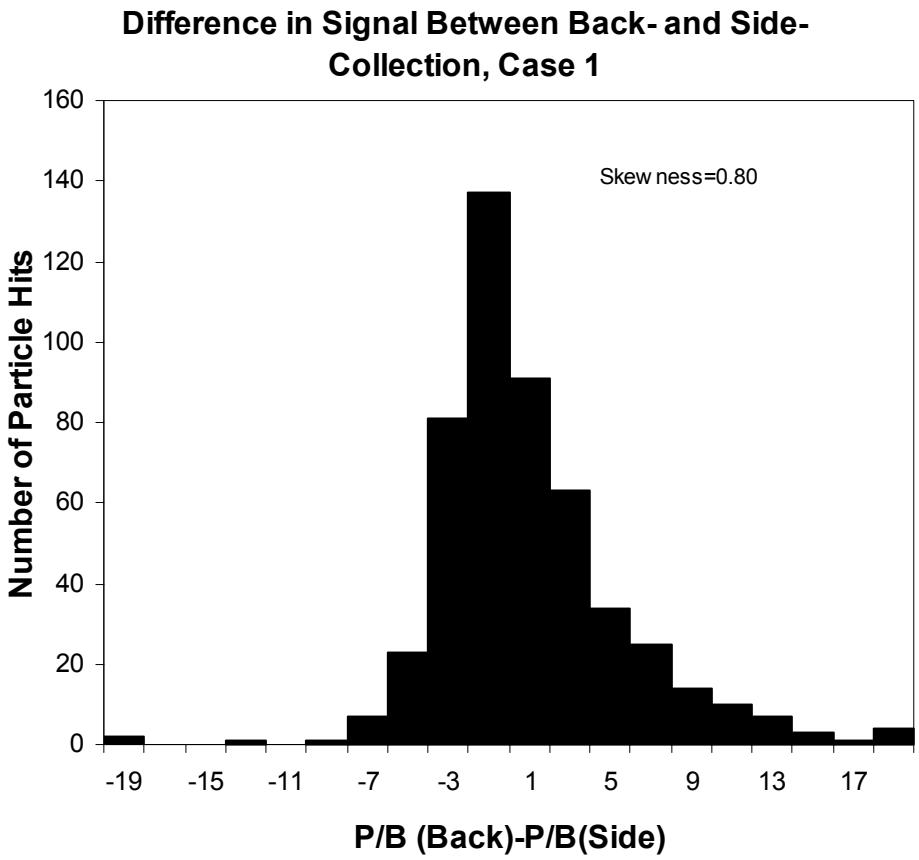
Difference in Signal Between Back- and Side-Collection, Case 1
Skew ness=0.80
Number of Particle Hits
160
140
120
100
80
60
40
20
0
-19
-15
-11
-7
-3
1
5
9
13
17
P/B (Back)-P/B(Side)

Figure 5 (a)

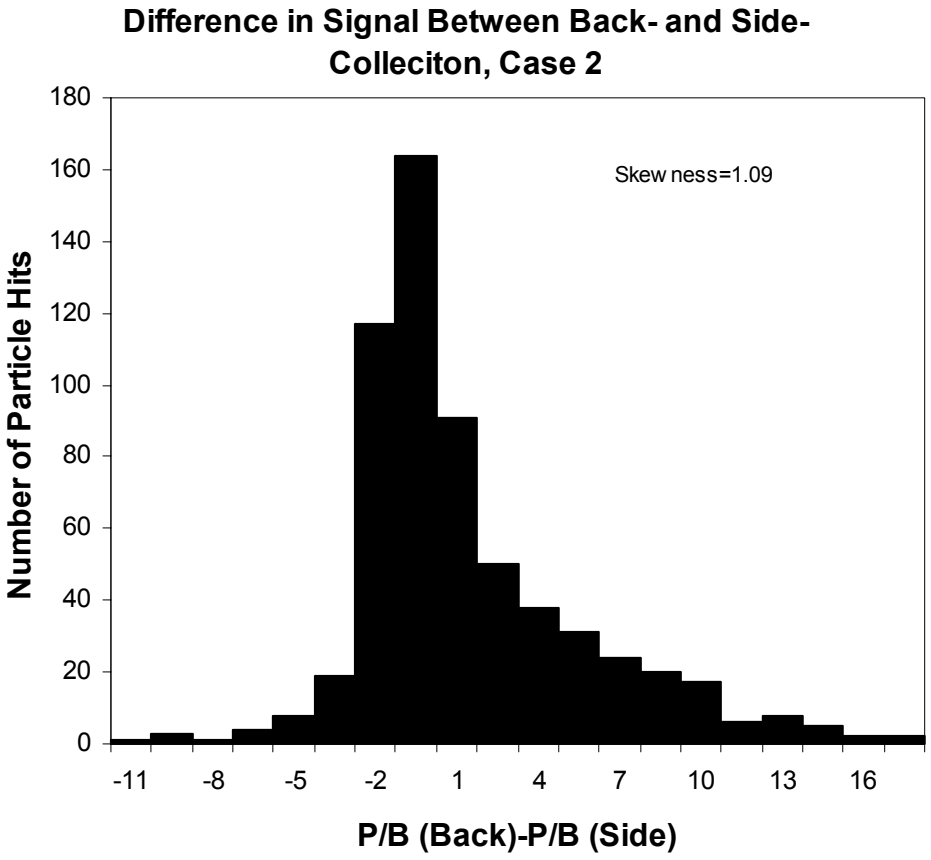
Difference in Signal Between Back- and Side-Colleciton, Case 2
Skew ness=1.09
Number of Particle Hits
P/B (Back)-P/B (Side)
180
160
140
120
100
80
60
40
20
0
-11
-8
-5
-2
1
4
7
10
13
16

Figure 5 (b)

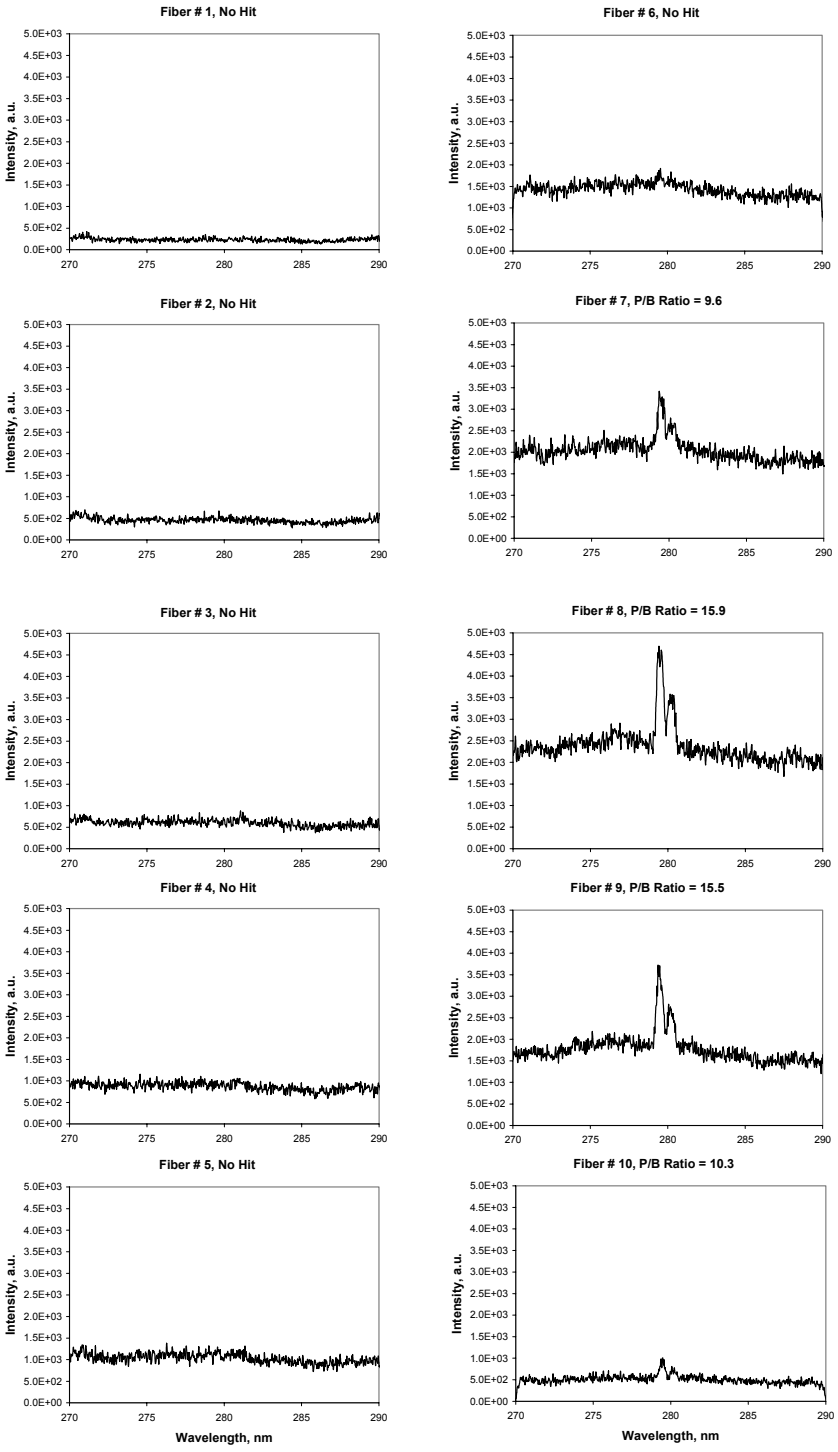
Fiber # 1, No Hit
Fiber # 6, No Hit
Fiber # 2, No Hit
Fiber # 7, P/B Ratio = 9.6
Fiber # 3, No Hit
Fiber # 8, P/B Ratio = 15.9
Fiber # 4, No Hit
Fiber # 9, P/B Ratio = 15.5
Fiber # 5, No Hit
Fiber # 10, P/B Ratio = 10.3
Intensity, a.u.
Wavelength, nm
5.0E+03
4.5E+03
4.0E+03
3.5E+03
3.0E+03
2.5E+03
2.0E+03
1.5E+03
1.0E+03
5.0E+02
0.0E+00
270
275
280
285
290

Figure 6

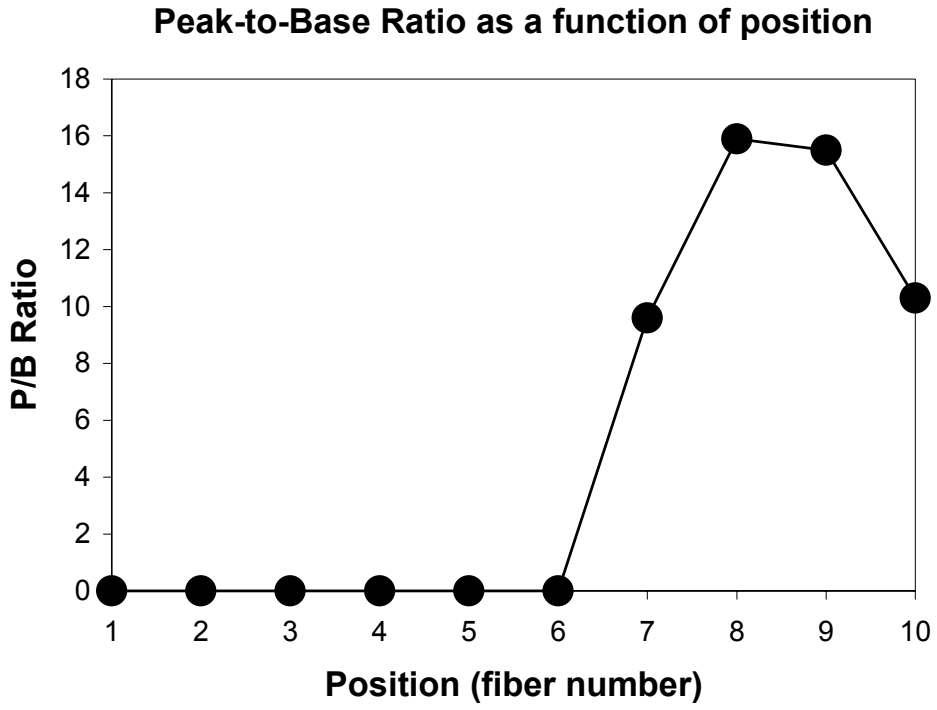
Peak-to-Base Ratio as a function of position
P/B Ratio
18
16
14
12
10
8
6
4
2
0
1
2
3
4
5
6
7
8
9
10
Position (fiber number)

Figure 7

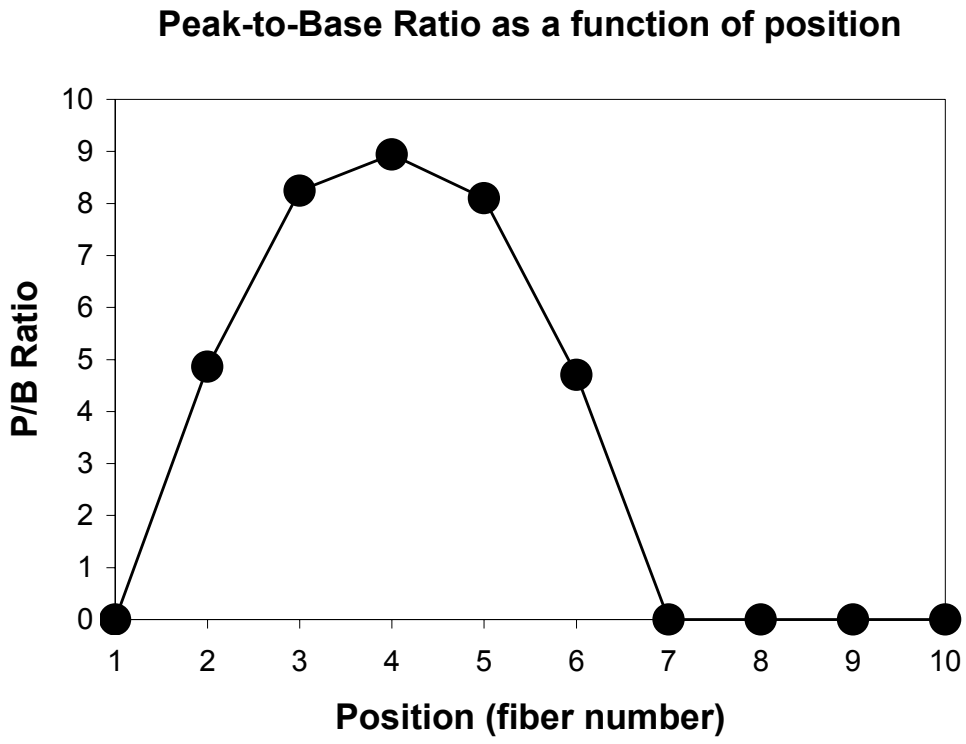
Peak-to-Base Ratio as a function of position
P/B Ratio
0
1
2
3
4
5
6
7
8
9
10
1
2
3
4
5
6
7
8
9
10
Position (fiber number)

Figure 8

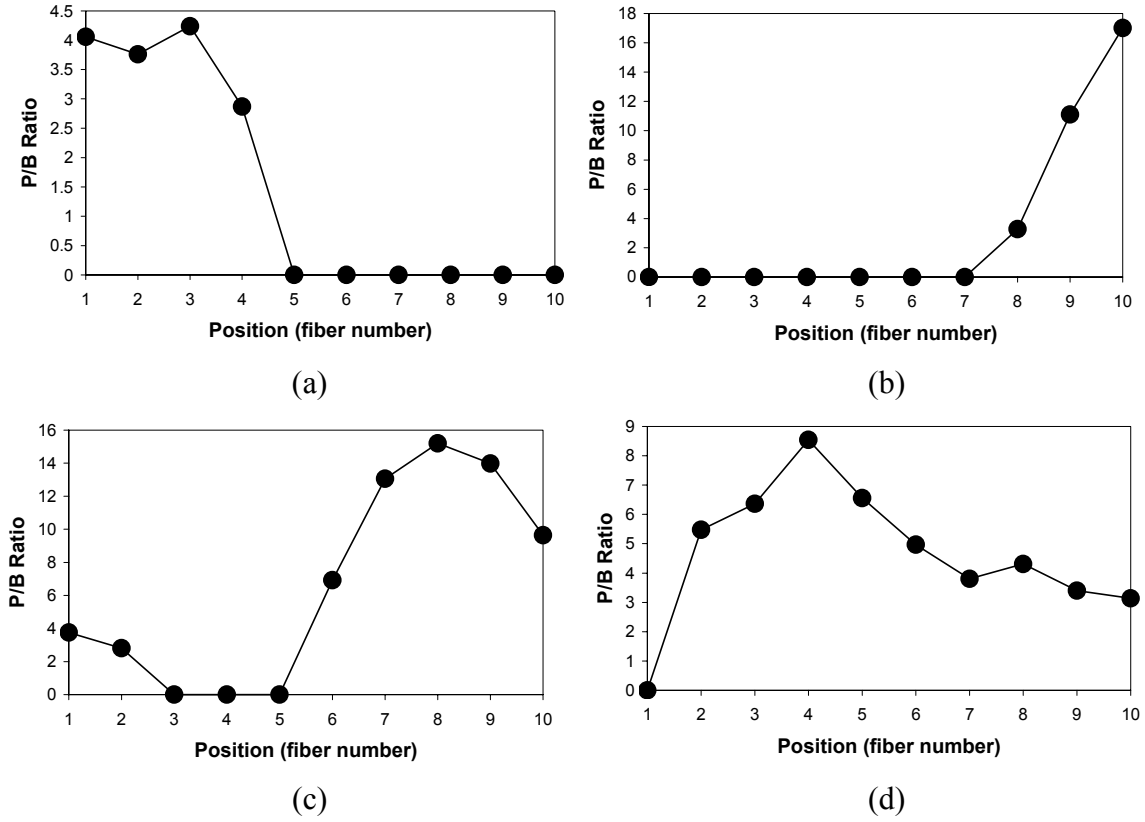


Figure 9

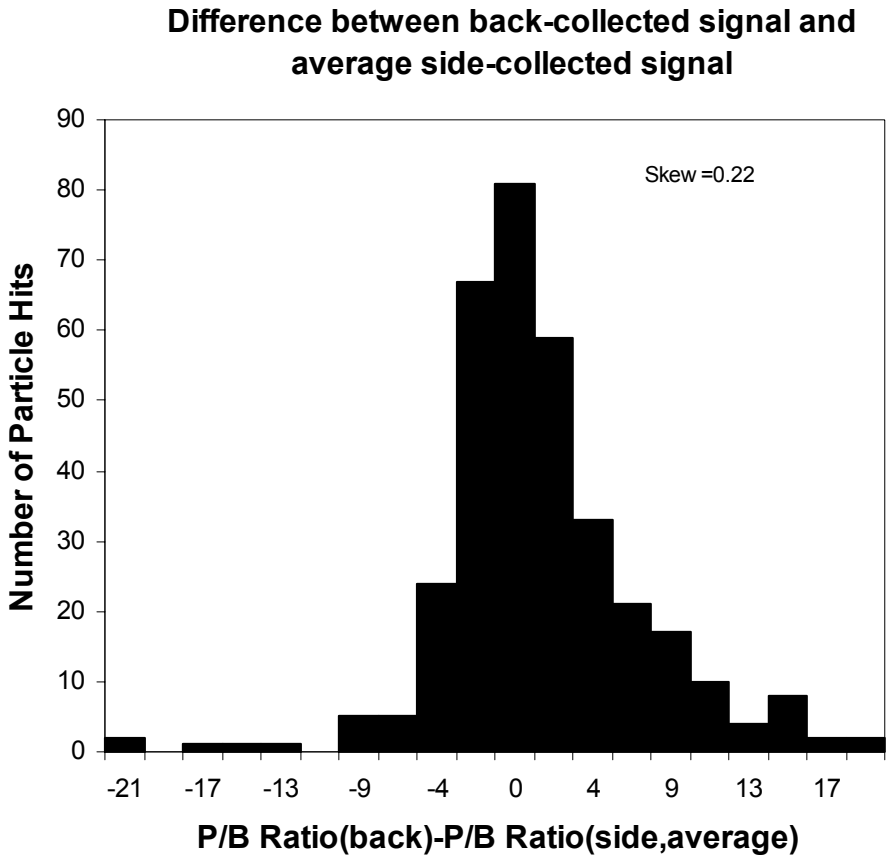
Difference between back-collected signal and average side-collected signal
Skew =0.22
Number of Particle Hits
90
80
70
60
50
40
30
20
10
0
-21
-17
-13
-9
-4
0
4
9
13
17
P/B Ratio(back)-P/B Ratio(side,average)

Figure 10 (a)

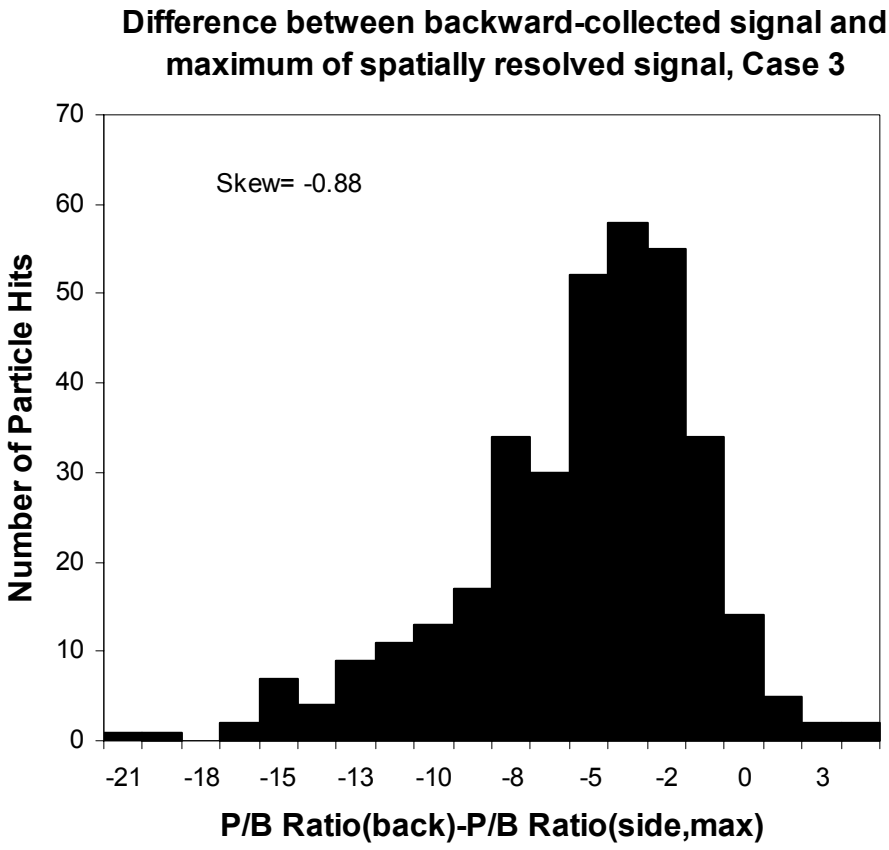
Difference between backward-collected signal and maximum of spatially resolved signal, Case 3
Skew= -0.88
Number of Particle Hits
70
60
50
40
30
20
10
0
-21
-18
-15
-13
-10
-8
-5
-2
0
3
P/B Ratio(back)-P/B Ratio(side,max)

Figure 10 (b)